CONF-9410216--10

Reactor Pressure Vessel Structural Integrity Research

W. E. Pennell and W. R. Corwin
Oak Ridge National Laboratory*
Oak Ridge, TN 37831

Summary

Development continues on the technology used to assess the safety of irradiation-embrittled nuclear reactor pressure vessels (RPVs) containing flaws. Fracture mechanics tests on RPV steel, coupled with detailed elastic-plastic finite-element analyses of the crack-tip stress fields, have shown that (1) constraint relaxation at the crack tip of shallow surface flaws results in increased data scatter but no increase in the lower-bound fracture toughness, (2) the nil ductility temperature (NDT) performs better than the reference temperature for nil ductility transition (RT_{NDT}) as a normalizing parameter for shallow-flaw fracture toughness data, (3) biaxial loading can reduce the shallow-flaw fracture toughness, (4) stress-based dual-parameter fracture toughness correlations cannot predict the effect of biaxial loading on shallow-flaw fracture toughness because in-plane stresses at the crack tip are not influenced by biaxial loading, and (5) an implicit strain-based dual-parameter fracture toughness correlation can predict the effect of biaxial loading on shallow-flaw fracture toughness. Experimental irradiation investigations have shown that (1) the irradiation-induced shift in Charpy V-notch vs temperature behavior may not be adequate to conservatively assess fracture toughness shifts due to embrittlement, and (2) the wide global variations of initial chemistry and fracture properties of a nominally uniform material within a pressure vessel may confound accurate integrity assessments that require baseline properties.

1 Introduction

Regulatory requirements limit the permissible accumulation of irradiation damage in the material of a reactor pressure vessel (RPV). Irradiation damage limits are set such that required fracture prevention margins are maintained throughout the nuclear plant licensed operating period. Regulatory requirements are based on fracture mechanics technology and utilize materials aging data drawn from mandatory reactor vessel irradiation damage surveillance programs.

In recent years it has become evident that a number of nuclear plants will exceed the regulatory limits on irradiation damage to the reactor vessel material before the end of their current operating license period.[1] One result from this development is that several nuclear industry organizations have gained experience in the application of fracture margin assessment technology. This experience has resulted in the identification of a number of issues with the technology in its present form. Data from irradiation testing programs, operating plant surveillance programs, and large-scale fracture technology validation tests have identified additional issues. The Nuclear Regulatory Commission (NRC)-funded Heavy-Section Steel Technology (HSST) and Heavy-Section Steel Irradiation (HSSI) Programs at Oak Ridge National Laboratory (ORNL) are performing the research required to resolve these issues and further develop and refine the fracture margin assessment technology.

This paper presents a brief overview of some of the research programs implemented to resolve the issues just identified. Elements of the HSST Program concerned with shallow-flaw and biaxial loading effects on fracture toughness are described. Application of results from these program elements to the evaluation of stress-based dual-parameter fracture toughness correlations and the development of an implicit strain-based dual-parameter correlation are reviewed. The HSSI Program elements concerned with the experimental investigation of irradiation effects on materials are presented. Results are reviewed from a study in which data from these experimental investigations were used to assess the adequacy of Charpy V-notch (CVN) vs temperature behavior as an indicator of the effects of neutron-irradiation-embrittlement of RPV steels.

*Research sponsored by Office of Nuclear Regulatory Research, U.S. Nuclear Regulatory Commission under Interagency Agreements 1886-8011-9B and 1886-8109-8L with the U.S. Department of Energy under contract DE-AC05-84OR21400 with Martin Marietta Energy Systems, Inc.

DISCLAIMER

DISCLAIMER

Portions of this document may be illegible in electronic image products. Images are produced from the best available original document.

2 HSST Program Research

Pressurized-thermal-shock (PTS) loading produces biaxial pressure and thermal stress fields in an RPV wall. Thermal stresses are highest adjacent to the inner surface of the vessel where the effects of irradiation embrittlement and transient temperatures combine to produce the maximum reduction in the material fracture toughness. The net result of this combination of conditions is that the majority of crack initiations predicted originate from shallow flaws located on the inner surface of the vessel. The dominant influence of shallow surface flaws generates a need for an experimental investigation of (1) the effect of reduced crack-tip constraint on the material fracture toughness associated with shallow flaws and (2) the effect of prototypical biaxial stress states on the material shallow-flaw fracture toughness, coupled with (3) development and validation of dual-parameter correlations that can be used to predict the material fracture toughness associated with shallow flaws in a biaxial stress field.

2.1 Shallow-Flaw Fracture Toughness

Fracture toughness tests have been performed on single-edge-notch-bending (SENB) test specimens using both deep (a/W = 0.5) and shallow (a/W = 0.1) flaws.[2,3] Beam specimens used in these tests are shown in Figs. 1 and 2. The beams tested by ORNL (Fig. 1) were fabricated from A 533 B material and were nominally 100 mm (4 in.) deep. Beams with a 230-mm-square (9-in.) cross section (Fig. 2) were cut from the RPV from a cancelled nuclear plant and tested, under an HSST Program subcontract, by the National Institute for Standards and Technology (NIST). The inner-surface stainless steel cladding remained in place on the large-scale test beams tested by NIST, and the flaws were located in the RPV longitudinal welds. Additional shallow-flaw fracture toughness data for A 533 B material were generated by the Fatigue and Fracture Branch of the Naval Surface Warfare Center (NSWC) in Annapolis, Maryland.[4] Material for the NSWC tests was heat treated to increase its yield stress. The NSWC tests were also conducted using large (B = 89 mm, W = 83 mm) SENB specimens. Use of large-scale beams permitted testing of shallow flaws with depths in the range identified as critical for PTS analysis. Data from Refs. 2–4 were all generated using large-scale SENB specimens fabricated from RPV steel. They can, therefore, be combined into deep- and shallow-flaw data sets.

Use of prototypical flaw depths reduced the uncertainties associated with extrapolation of shallow-flaw fracture toughness data for application to full-scale structures.

The reference temperature for nil-ductility transition (RT_{NDT}) is used as a normalizing parameter for fracture toughness data. The *American Society of Mechanical Engineers (ASME) Boiler and Pressure Vessel Code*[5] defines RT_{NDT} in terms of both the nil ductility temperature (NDT) and the temperature (T_{cv}) at which the lower-bound Charpy energy from three tests is not less than 68 J (50 ft·lb.). One of the temperatures (NDT or T_{cv}) will be the controlling temperature for RT_{NDT} in a given situation. Table 1 gives NDT, T_{cv}, and RT_{NDT} for each of the materials tested in the shallow-flaw program. Examination of the NDT and RT_{NDT} data in Table 1 reveals that a mix of governing conditions is contained within the data sets from NSWC, ORNL, and NIST. NDT and RT_{NDT} are identical, within a data set, in the NSWC tests, and in the ORNL tests on the Combustion Engineering (CE) material. RT_{NDT} is higher than NDT for the ORNL tests on material from HSST Plate 13B and for the NIST tests on weld metal, indicating that T_{cv} controlled RT_{NDT} in these cases.

Deep- and shallow-flaw fracture toughness data generated in these tests are plotted as a function of the normalizing temperature RT_{NDT} in Figs. 3 and 4, respectively. Open points and solid points in these plots represent data from material where RT_{NDT} was controlled by NDT and T_{cv}, respectively. The deep-flaw open and solid data points in Fig. 3 form a homogeneous group, indicating that RT_{NDT} is a satisfactory normalizing parameter for deep-flaw data. In contrast, the open- and solid-point shallow-flaw data in Fig. 4 appear to belong to two separate families, with quite separate lower-bound curves. The apparent existence of two separate families of data for a single material calls into question the adequacy of RT_{NDT} as a normalizing parameter for the shallow-flaw fracture toughness of A 533 B plate and weld material.

Tests used to determine NDT and T_{cv} are fundamentally different in character, and this difference could influence the interpretation, shown in Fig. 4, of the shallow-flaw fracture toughness data. This problem can be eliminated by adopting a common basis for the normalizing parameter used to compare the data sets. This has been done in Fig. 5, where NDT has been used as the normalizing parameter for all data points. Figure 5 shows that the shallow-flaw fracture toughness data from all sources form a homogeneous population when plotted as a function of T – NDT. A single curve defines the lower bound to the shallow-flaw fracture toughness data sets. A comparison of Figs. 3 and 5 shows that the lower-bound curves for the deep- and shallow-flaw data are similar, but the mean fracture toughness and scatter of data are significantly higher for shallow flaws than for deep flaws.

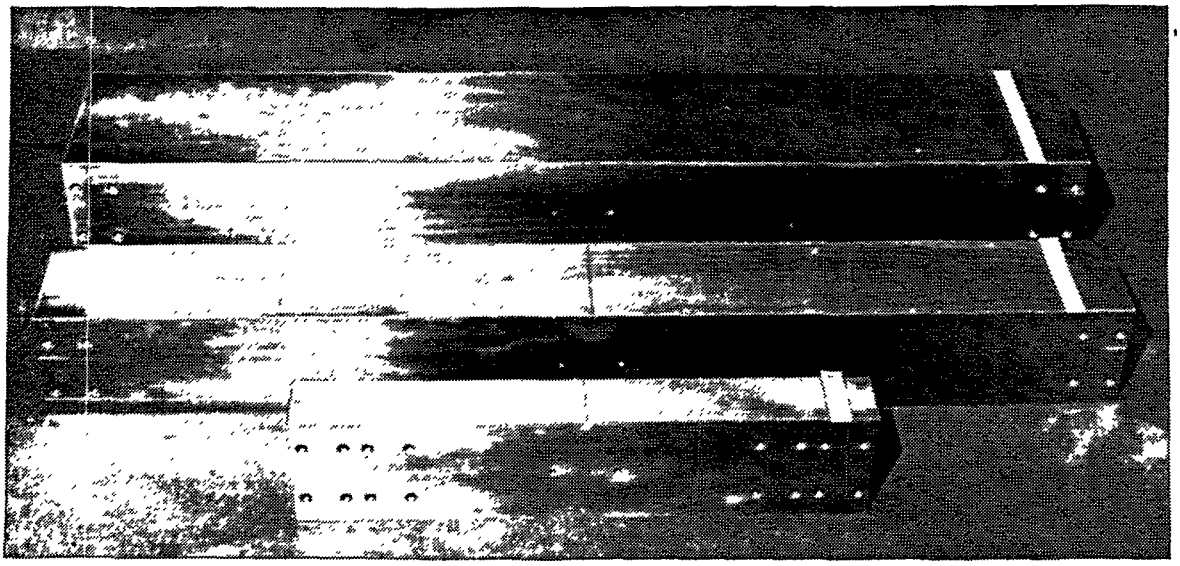

Figure 1 The 100-mm deep beams were used in the shallow-flaw test program to permit full-scale testing of surface flaws having depths in the range that PTS analysis has shown to be the controlling range for crack initiation.

Figure 2 A limited number of full-scale beam specimens used in shallow-flaw test program were cut from the shell of an RPV from a cancelled nuclear plant.

Table 1 Reference temperatures for material used in the shallow-flaw SENB and cruciform test specimens

Laboratory	Specimen type	Material	NDT [°C (°F)]	T_{cv} [°C (°F)]	RT_{NDT} [°C (°F)]
NSWC	SENB	Plate 11 (surface)	–7 (19)	24 (76)	–7 (19)
NSWC	SENB	Plate 11 (1/4 thickness)	4 (39)	31 (88)	4 (39)
ORNL	SENB	C-E plate	–35 (–31)	–17 (1)	–35 (–31)
ORNL	SENB	Plate 13B	–30 (–22)	18 (65)	–15 (5)
ORNL-NIST	SENB	V. weld	–50 (–58)	10 (50)	–23 (–10)
ORNL	BIAX	C-E plate	–35 (–31)	–17 (1)	–35 (–31)

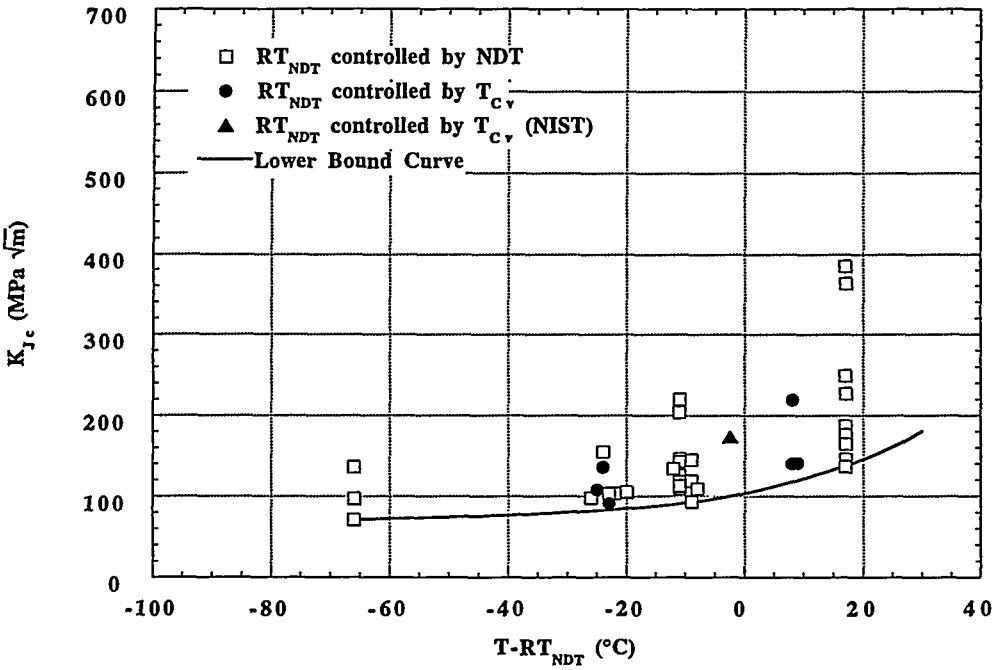

Figure 3 The parameter-controlling RT_{NDT} has no significant effect on the distribution of K_{Jc} vs $T - RT_{NDT}$ data points from the deep-crack SENB A 533 B specimens. A single curve adequately defines the lower bound for the combined data set.

2.2 Biaxial Loading Effects on Shallow-Flaw Fracture Toughness

A typical biaxial stress field produced by PTS transient loading is shown in Fig. 6, together with a constant-depth shallow surface flaw. One of the principal stresses is seen to be aligned parallel to the crack front. There is no counterpart of this far-field out-of-plane stress in the shallow-flaw fracture toughness tests previously described. The far-field out-of-plane stress has the potential to increase stress triaxiality (constraint) at the crack tip and thereby reduce some of the fracture toughness elevation associated with shallow flaws. The HSST biaxial test program was instituted to investigate this effect.

A cruciform test specimen was developed at ORNL to investigate the effects of biaxial loading on the shallow-flaw fracture toughness of pressure vessel steels.

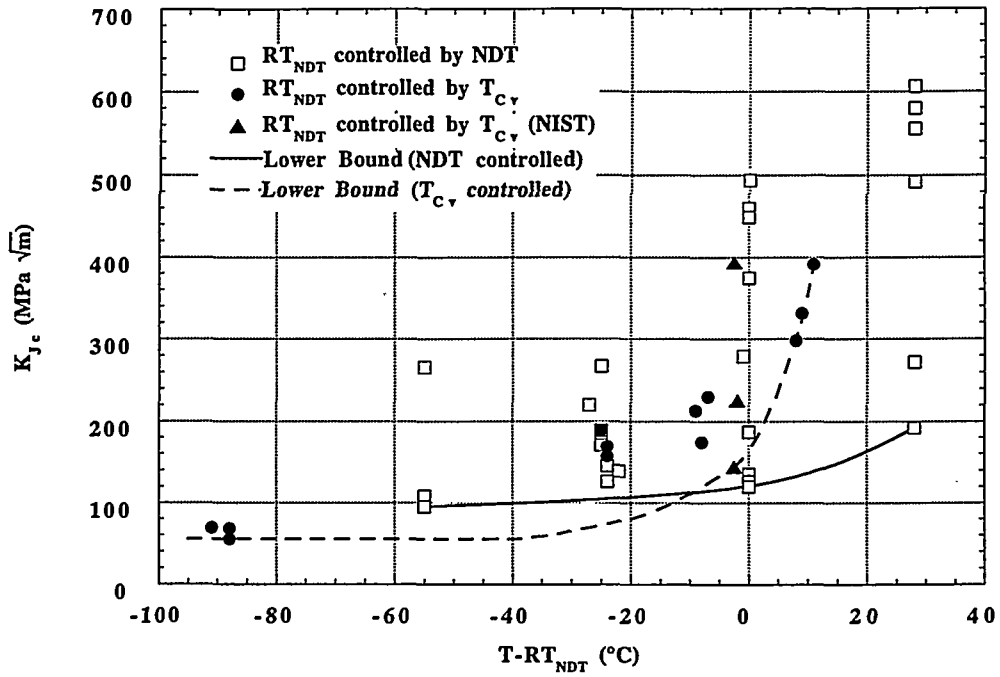

Figure 4 Shallow-flaw fracture toughness data for A 533 B plate and weld material fall into two distinct groups when plotted as a function of the normalizing parameter T – RT_{NDT}. The groups are characterized by the parameter-controlling RT_{NDT} (NDT or T_{CV}).

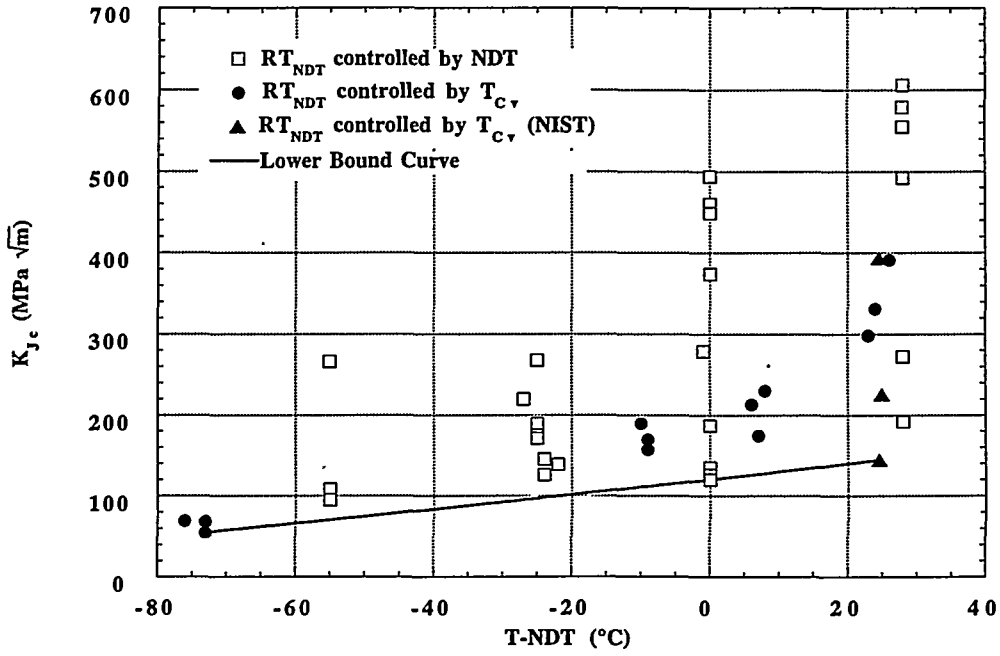

Figure 5 Shallow-flaw fracture toughness data for A 533 B plate and weld material form a single homogeneous group when plotted as a function of the normalizing parameter T – NDT. The lower-bound curve of this data set is similar to that of the deep-flaw data set, but the shallow-flaw data set shows an increase in both mean toughness and data scatter.

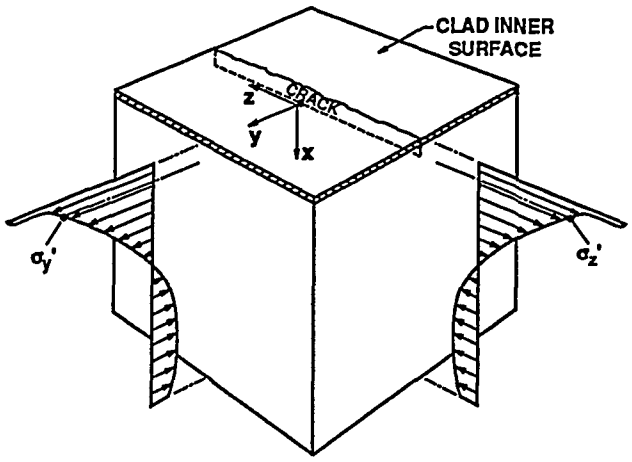

Figure 6 **PTS loading produces biaxial stresses in an RPV wall with one of the principal stresses aligned parallel with the tip of a constant-depth shallow surface flaw.**

Conceptual features of the specimen are shown in Fig. 7. The specimen design is capable of reproducing a linear approximation of the nonlinear biaxial stress distribution shown in Fig. 6. The cruciform design, coupled with a statically determinate load reaction system, permits the specimen to be loaded in either uniaxial (4-point bending) or biaxial (8-point bending) configurations. Tests of nominally identical specimens can thus be performed with the level of stress biaxiality as the only test variable.

An initial series of biaxial tests has been completed using test specimens fabricated from a single heat of A 533 B material. The biaxial load ratio is defined as P_T/P_L, where P_T is the total load applied to the transverse beam arms, and P_L is the total load applied to the longitudinal arms. Tests were run with P_T/P_L ratios of 0, 0.6, and 1. Details of those tests have been extensively reported[6,7] and will not be repeated here. K_{Jc} data from the biaxial tests are shown in Fig. 8, plotted as a function of the biaxiality ratio P_T/P_L. The plot shows a decrease in the lower-bound shallow-flaw fracture toughness with increasing biaxiality ratios. The data also indicate a trend of decreasing data scatter at a stress ratio of 0.6 when compared with the data scatter observed in both the uniaxial ($P_T/P_L = 0$) SENB shallow-flaw tests (see Fig. 5) and the biaxial shallow-flaw tests at a P_T/P_L loading biaxility ratio of 1.

2.3 Development of a Dual-Parameter Fracture Toughness Correlation

Dual-parameter fracture toughness corrections and correlations have been proposed to provide a quantitative assessment of effect of reduction of crack-tip constraint on fracture toughness. These include the J-A_{cr} fracture toughness correction proposed by Dodds, Anderson, and Kirk[8] and the J-Q dual-parameter fracture toughness correlation proposed by O'Dowd and Shih.[9,10] These dual-parameter fracture-toughness corrections and correlations share a common feature because they each utilize the effect of crack-tip constraint on in-plane stresses at the crack-tip to infer the effect of constraint on fracture toughness.

In the J-Q fracture toughness correlation, Q defines the departure of the stress-state-dependent opening-mode stress distribution on the crack plane from the opening-mode stress distribution derived by Hutchinson[11] and Rice and Rosengren[12] (HRR) for a highly constrained crack tip. Richie, Knott, and Rice (RKR) have proposed a criterion relating the critical value of the crack-tip opening-mode tensile stress at a critical distance from the crack tip for the onset of cleavage fracture in mild steel under plane-strain constraint conditions.[13] The J-Q fracture toughness correlation uses the RKR concept of a critical opening-mode tensile stress, together with the influence of constraint on opening-mode stresses represented by the parameter Q, to correlate the effect of crack-tip constraint on fracture toughness.

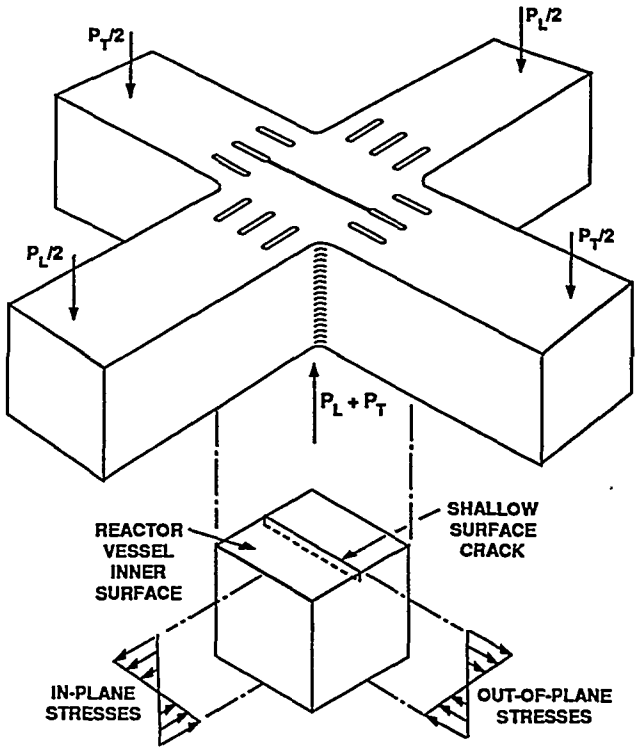

Figure 7 **Conceptual features of the cruciform shallow-flaw biaxial fracture toughness test specimen.**

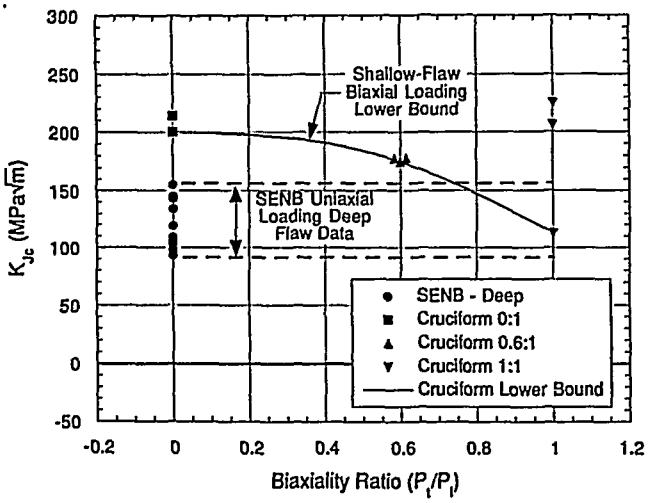

Figure 8 Data from a single heat of A 533 B steel tested at T – NDT = –10°C indicate that biaxial loading reduces the lower-bound transition-range shallow-flaw fracture toughness.

Prior investigations of biaxial loading effects have concluded that out-of-plane biaxial loading had no effect on in-plane stresses at the crack tip[14,15] but did influence the width of the crack-tip plastic zone in the direction of crack propagation. Recent elastic-plastic finite-element analyses of the ORNL biaxial specimen, performed by B. R. Bass and J. W. Bryson using a model with highly refined treatment of the crack-tip region (see Fig. 9), have confirmed these conclusions. The Bass-Bryson analyses have further confirmed that the stress-based J-A_{cr} constraint correction cannot predict the observed effects of biaxial loading on shallow-flaw fracture toughness. The HSST Program has, therefore, investigated the utility of strain-based constraint-effects technology.

A review of the facts supporting development of a strain-based dual-parameter correlation for transition range fracture toughness is appropriate at this point. Clausing[16] showed that the plane-strain ductility of structural steels increases rapidly over a relatively small temperature range, corresponding with the fracture toughness transition temperature range. Clausing related the decrease in toughness associated with increased strength to the associated decrease in plane-strain ductility. Barsom[17] and Merkle[18] developed expressions for K_{Ic} based upon plane-strain ductility. The expressions of Refs. 17 and 18 produced K_{Ic} predictions that matched the test data for temperatures in the transition range. Weiss[19] developed an equation for fracture toughness based upon the stress-state-dependent material fracture strain. An adaptation of the Weiss equation was used in the scoping analysis of Ref. 15 to determine the potential impact of biaxial loading on fracture toughness. The scoping analysis of Ref. 15 predicted a K_{JcB}/K_{JcU} ratio of 0.47 for equibiaxial loading, where K_{JcB} and K_{JcU} are values of K from J for biaxial and uniaxial loading conditions, respectively. This compares with the lower-bound K_{JcB}/K_{JcU} ratio of 0.56 obtained in tests (see Fig. 8) with equibiaxial and uniaxial loading. Similarity of the predicted and measured K_{JcB}/K_{JcU} values is supportive of a strain-based fracture toughness correlation. Fractographic data from examinations of broken fracture specimens[7,20] provide further support for a strain-based fracture toughness correlation. The fractographic data indicate that many crack initiation sites are located in the region of the crack-tip process zone where strain is increasing, but stress is decreasing, with increasing applied K_J.

Tetleman and McEvily (T&M)[21] postulate that plastically induced fracture initiates in a ligament immediately adjacent to the blunted crack tip when the ligament strain reaches the fracture strain (e_f) of the material. They approximate the ligament length as twice the root radius of the blunted crack tip. The T&M fracture criterion can be interpreted as a limiting condition for energy absorption by inelastic deformation of the crack-tip material. It should be possible, therefore, to determine the effects of constraint on fracture toughness by analyzing the response of the crack-tip material to increasing load and determining the radius of the blunted crack tip at which the crack-tip ligament strain reaches e_f. The blunted crack tip has a free surface. The fracture strain (e_f) for material immediately adjacent to the crack tip is, therefore, the plane-strain fracture strain determined by Clausing.[16]

Direct implementation of the strain-based constraint-effects methodology just described would require a computationally intensive, finite strain, elastic-plastic finite-element analysis. This analysis would be required to

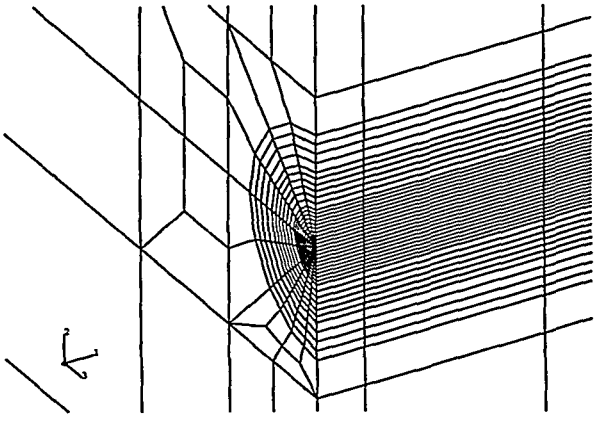

Figure 9 Detail of the crack-tip region of the cruciform specimen finite element model.

determine the crack-tip radius corresponding with the generation of strains equal to the fracture strain in material immediately adjacent to the blunted crack tip. Fortunately, the crack-tip plastic deformation is approximately equal to the plastic displacement $e_y \cdot R$, where e_y is the material yield strain and R is the width of the crack-tip plastic zone in the crack plane.[21] A strain-based constraint effects methodology can, therefore, be based on the effects of crack-tip constraint on R. The parameter R can be calculated accurately in a small strain analysis.

The influence of biaxial loading on the growth of the plastic zone width (R) in response to increasing load is shown in Fig. 10. Results plotted in Fig. 10 were taken from analyses performed by Bass and Bryson using the analysis model of Fig. 9, with the material stress-strain properties shown in Fig. 11. The curves of Fig. 10 show that biaxial loading has the effect of inhibiting the growth of the plastic zone width R. In the case of the $P_T/P_L = 0.6$ loading, the inhibiting effect is present over the entire loading range. In the case of the $P_T/P_L = 1.0$ loading, however, growth of the plastic zone width is inhibited up to an applied loading of ~1000 MPa (150 kips), where rapid growth occurs because of the onset of uncontained yielding of the specimen. The curve for $P_T/P_L = 1.0$ loading becomes similar to the curve for uniaxial loading at load levels beyond those shown in Fig. 10. This effect of uncontained yielding may explain why some researchers, using small test specimens in which uncontained yielding was unavoidable, have reported no effects of biaxial loading on fracture toughness. The influence of biaxial loading on R depicted in Fig. 10 would indicate that a strain-based constraint-effects model, using R as a second parameter, should predict an effect of biaxial loading on fracture toughness.

Biaxial fracture toughness (K_{Jc}) values from Fig. 8 are shown plotted as a function of the natural logarithm of the plastic zone width [ln(R)] in Fig. 12. The parameter ln(R) was used rather than R because the data conformed to a simple straight-line relationship when presented in this form. A $\pm$ 22-MPa$\sqrt{m}$ ($\pm$20-ksi$\sqrt{in.}$) uncertainty band accomodates scatter in the, admittedly small, data set. The uncertainty band in Fig. 12 represents the fracture toughness locus for the test material for a normalized temperature (T – NDT) of – 10°C. A series of fracture toughness loci would have to be generated to cover the range of normalized temperatures of interest in RPV safety evaluations.

K_{Jc} – ln(R) loading trajectories from the Bass-Bryson analyses are shown in Fig. 13, superimposed on the fracture toughness locus from Fig. 12. Note that each biaxial loading ratio produces a unique K_{Jc} – ln(R) trajectory. Intersection of the K_{Jc} – ln(R) loading trajectory for a particular loading biaxiality ratio with the fracture

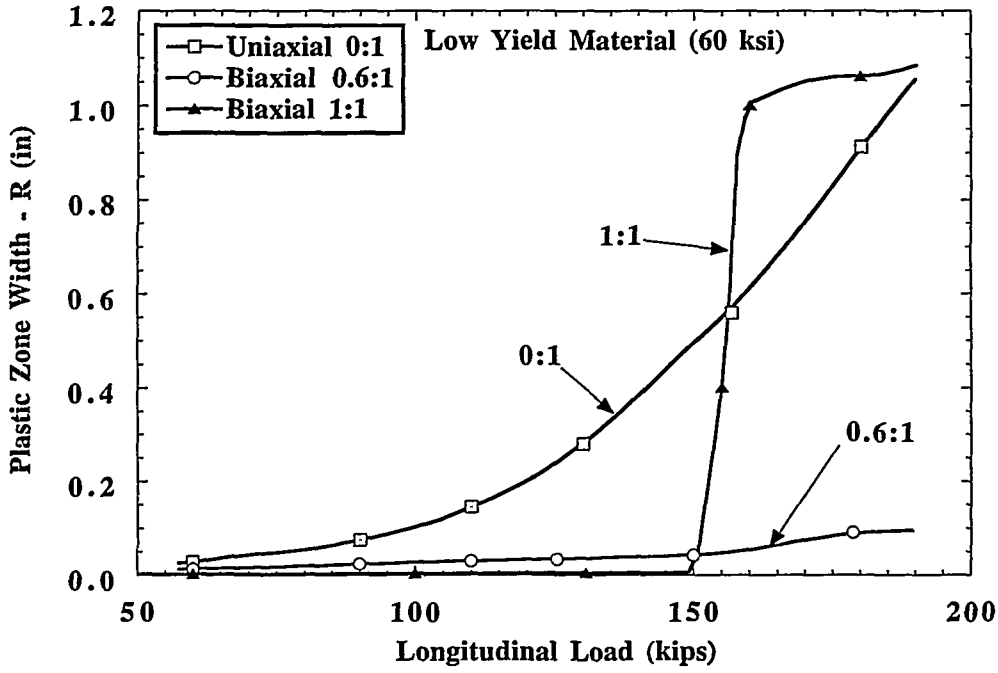

Figure 10 The rate of increase of the width (R) of the crack-tip plastic zone in the direction of crack propagation is directly related to the biaxial loading ratio P_T/P_L.

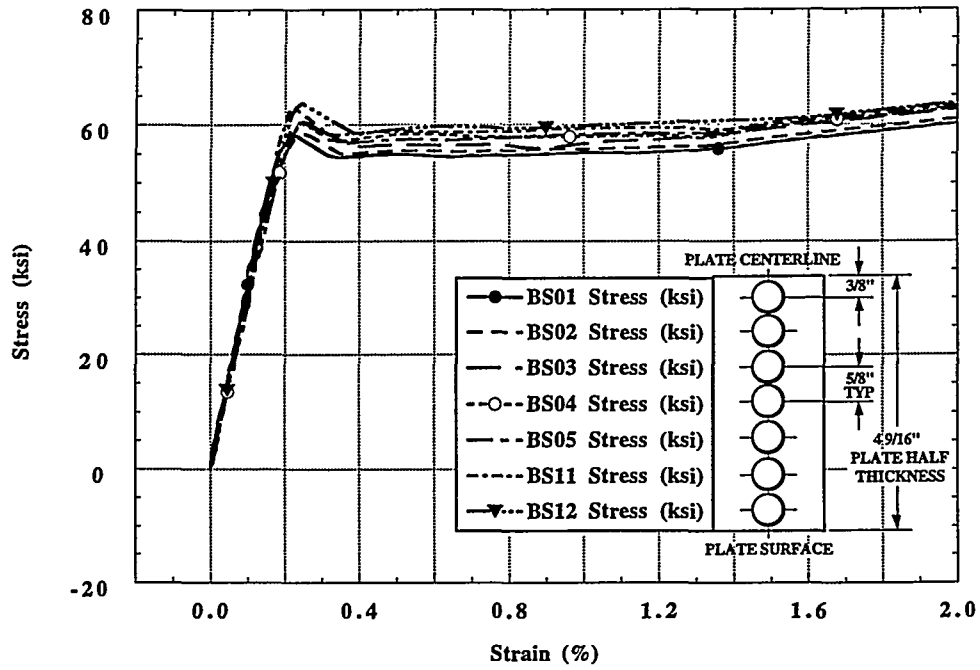

Figure 11 The C-E A 533 B Grade 1 plate material used to fabricate the biaxial test specimens exhibits an abrupt transition from linear-elastic behavior followed by significant Lüders straining, before the onset of strain hardening.

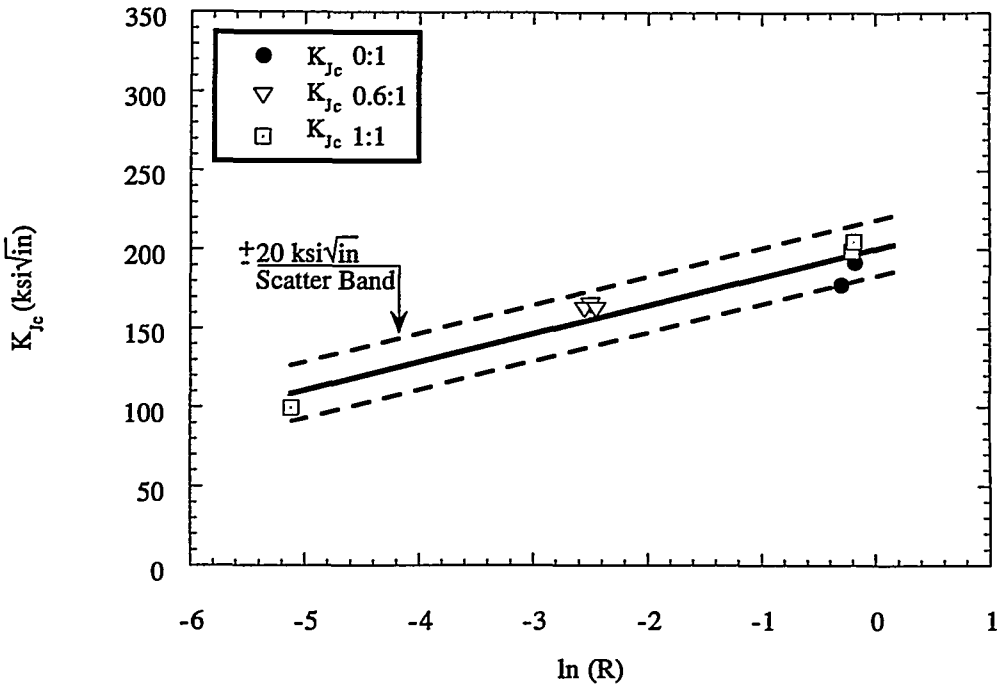

Figure 12 Test data and analysis results for the biaxial specimen are combined to define a K_{Jc}-ln(R) shallow-flaw fracture toughness locus.

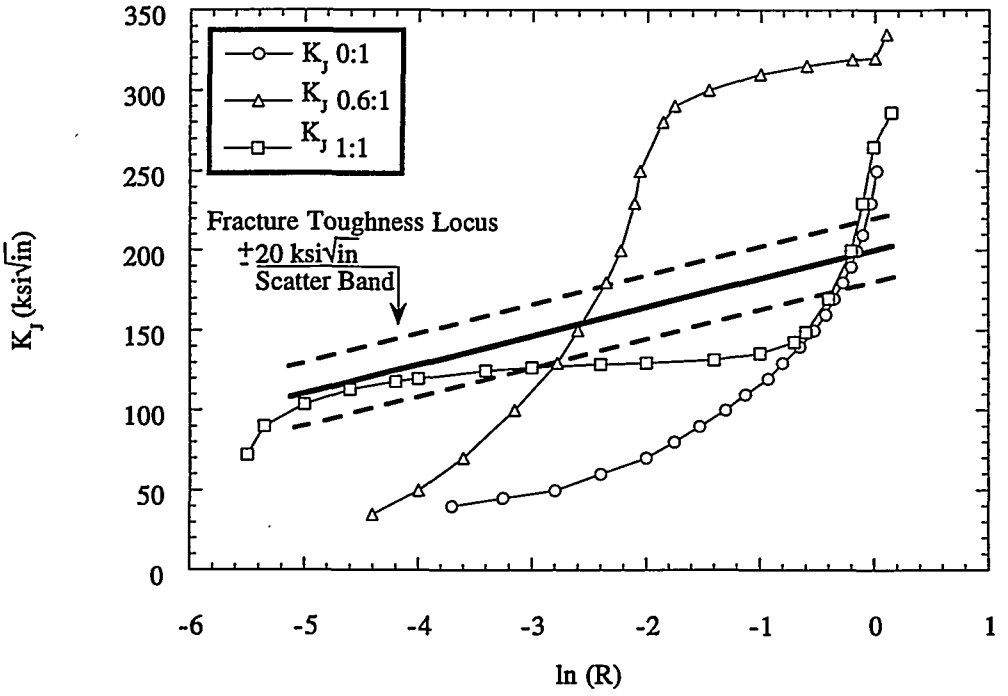

Figure 13 **K_{Jc}-ln(R) trajectories for the biaxial specimen predict unique K_{Jc} values for uniaxial and $P_T/P_L = 0.6$ loading, but both high and low K_{Jc} values are possible for the $P_T/P_L = 1.0$ loading because of the low yield stress of the material used for these tests.**

toughness locus predicts the range of fracture toughness values possible for that loading condition at a normalized temperature (T – NDT) of –10°C. The results summarized in Fig. 13 suggest that a strain-based K_{Jc} – ln(R) has the potential for development into a dual-parameter fracture toughness correlation capable of representing the effects of crack-tip constraint on the fracture toughness of RPV steels, including the effects of stress biaxiality.

Before leaving this topic, two important influences of the material stress-strain curve on the results presented above should be noted.

1. The onset of uncontained yielding has a pronounced effect on the loading trajectory for the $P_T/P_L = 1.0$ loading condition, causing it to intersect the fracture toughness locus at both low and high values of K_{Jc}. The low yield stress of the material used in this series of tests [σ_y = 414 MPa (60 ksi)] resulted in uncontained yielding in two of the $P_T/P_L = 1.0$ tests, giving biaxial test results that are similar to the uniaxial results. Analysis performed with a material yield stress of 621 MPa (90 ksi) did not show any effects of uncontained yielding with $P_T/P_L = 1.0$ over the loading range investigated.

2. Test data for A 533 B RPV steel, irradiated to fluences up to 5.5×10^{19} neutrons/cm^2 (E >1 MeV), showed that a sharply defined departure from linear-elastic behavior is present in both unirradiated and irradiated material tested at both very low and very high straining rates.[22] Inclusion of the sharply defined departure from linear-elastic behavior shown in Fig. 11 is essential to an accurate prediction of the effect of biaxial loading on the width R of the plastic zone. The effects of concern cannot be predicted using a power law approximation of the stress-strain curve.

3 HSSI Program Research

3.1 K_{Ic} Curve Shifts in High-Copper Welds

To account for the effects of neutron irradiation on toughness, the initiation and arrest fracture toughness curves as described in Sect. XI of the *ASME Boiler and*

Pressure Vessel Code are shifted upward in temperature without change in shape by an amount equal to the shift (plus a margin term) of the CVN impact energy curve at the 41-J (30-ft·lb) level. Such a procedure implies that the shifts in the fracture toughness curves are the same as those of the CVN 41-J energy level and that irradiation does not change the shapes of the fracture toughness curves.

The objectives of the HSSI Fifth and Sixth Irradiation Series are to determine the K_{Ic} and K_{Ia} curve shifts and shapes for two irradiated high-copper, 0.23 and 0.31 wt %, submerged-arc welds (72W and 73W, respectively). Irradiations were performed at 288°C (550°F) to average fluences of about 1.5×10^{19} neutrons/cm^2 (E > 1 MeV). Tests included tensile, CVN impact, drop-weight, and fracture toughness. Compact specimens up to 203 and 101 mm (8 and 4 in.) in thickness were tested in the unirradiated and irradiated conditions, respectively. The detailed results of testing have been presented previously.[23] For the CVN results, the 41-J (30-ft·lb) transition temperature shifts were 72 and 82°C (130 and 148°F), while the 68-J (50-ft·lb) shifts were 82 and 105°C (148 and 189°F) for welds 72W and 73W, respectively.

For those fracture specimens that met the American Society for Testing and Materials (ASTM) E399 criteria for a valid K_{Ic}, the K_{Ic} value is used in the analysis. For those specimens that exhibited curvature in the load-displacement record, indicative of plastic deformation and, perhaps, stable ductile tearing, the K_{Jc} value was used. To include both linear-elastic and elastic-plastic fracture mechanics calculations, data have been designated K_{cl} for cleavage fracture toughness. Figure 14 shows that an unexpectedly large number of cleavage pop-ins occurred in the irradiated data set. Of 156 unirradiated compact specimens, only 2 exhibited pop-ins, as compared to 36 pop-ins for the 110 irradiated specimens. To be conservative, only the initial pop-in is used here to determine cleavage fracture toughness for those specimens exhibiting pop-ins.

Linearized two- and three-parameter nonlinear regression analyses similar in form to the K_{Ic} curve in Sect. XI of the ASME Code gave fracture toughness temperature shifts, measured at the 100-MPa$\sqrt{m}$ (91- ksi$\sqrt{in.}$) level, of about 83 and 99°C (149 and 178°F) for 72W and 73W, respectively. The analyses show some decreases in slopes for the irradiated data for both welds. These decreases, however, are only about 4.1 and 6.9% for 72W and 73W, respectively, with large enough standard errors to imply a low statistical significance of the slope changes. For the combined data sets, with temperature normalized to RT_{NDT}, the differences are about 10, 15, and 17°C (18, 27, and 31°F) between the unirradiated and irradiated mean fracture toughness curves at K_{cl} values of 50, 100, and 200 MPa$\sqrt{m}$ (46, 91, and 182 ksi$\sqrt{in.}$), reflecting the average change in curve shape.

Figure 15 shows a plot of the irradiated fracture toughness data and various curves for 73W. The ASME K_{Ic} curve is shown for both the unirradiated and the irradiated conditions after shifting the curve upward. The dashed curves labeled 1–3 represent different methods for shifting the K_{Ic} curve. The curve labeled 4 represents the ASME K_{Ia} curve shifted upward in temperature equal to the Charpy 41-J (30-ft·lb) shift (TT41). The curve labeled 5 is the five- percentile curve produced using the method of Wallin.[24] For 72W, the data are bounded by the TT41 + margin curve and the K_{cl} curve, but neither of these curves quite bound all the data for 73W. The margin is 15.6°C (28°F) as defined in Regulatory Guide 1.99 (Rev. 2) assuming credible surveillance data. The K_{Ia} curve is shown to allow for comparison of that curve with the shifted K_{Ic} curves, especially regarding curve shape, in view of the observation that the irradiated K_{cl} curves for these two welds appear to have exhibited some shape change after irradiation. Figure 16 shows all the irradiated fracture toughness data for 72W and 73W plotted vs temperature normalized to the RT_{NDT}. As shown in the figure, a total of eight data points fall below the ASME K_{Ic} curve. To bound all data, the dashed K_{Ic} curve must be shifted upward in temperature 18°C (32°F).

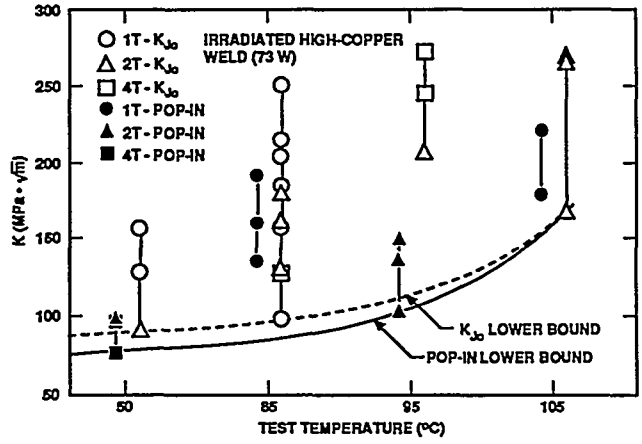

Figure 14 Test data for irradiated high-copper weld (73W) indicate that lower-bound fracture toughness curve reflecting pop-in test data differs very little from one derived from K_{Jc} data.

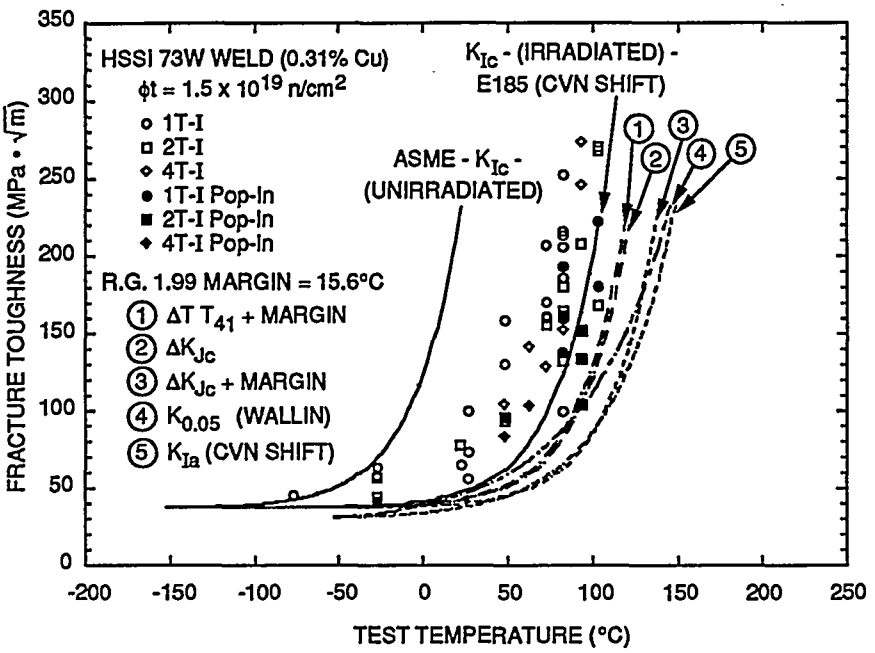

Figure 15 Fracture toughness, K_{cl}, vs test temperature for irradiated HSSI weld 73W. The ASME K_{Ic} curve for the unirradiated data is shown, as is the same curve after shifting it upward in temperature equal to the Charpy 41-J shift. The curves labeled 1, 2, and 3 represent the ASME curve shifted by the indicated criterion, where margin is 15.6°C. The K_{Ia} curve represents the ASME K_{Ia} curve shifted by the Charpy 41-J shift. The $K_{0.05}$ curve is the five-percentile curve for all the HSSI 72W and 73W combined data using the Wallin procedure.

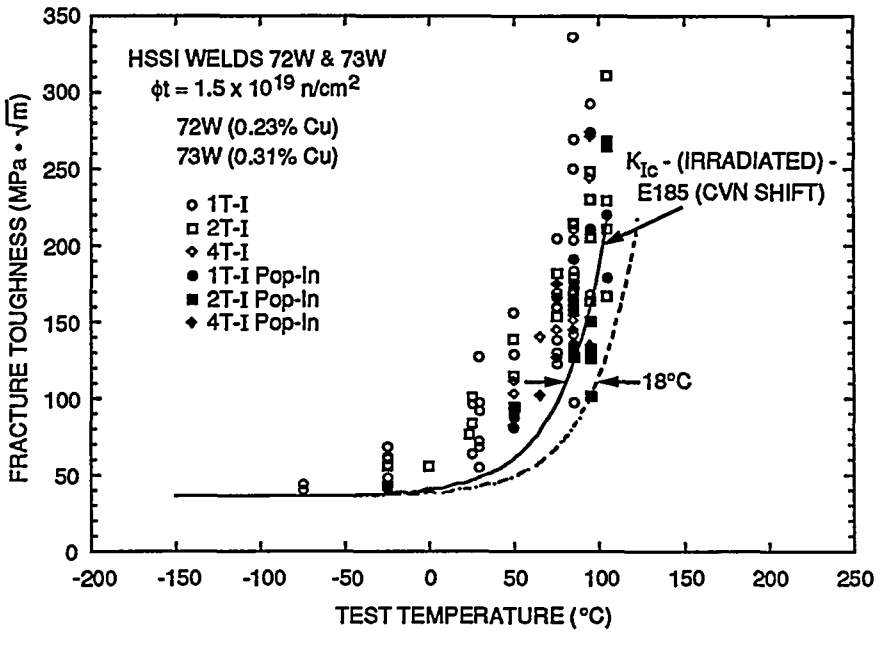

Figure 16 Fracture toughness, K_{cl}, vs normalized temperature, $T - RT_{NDT}$, for irradiated welds 72W and 73W. The dashed curve is the ASME curve shifted upward in temperature to just bound the irradiated data.

Observations from the HSSI Fifth and Sixth Irradiation Series included the irradiation-induced temperature shift. Statistical analyses and curve fitting showed that the temperature shifts at a fracture toughness of 100 MPa$\sqrt{m}$ (91 ksi$\sqrt{in.}$) were greater than those at a Charpy energy of 41 J (30 ft·lb) but were in good agreement with the Charpy 68-J (50-ft·lb) transition shifts. The 68-J temperature shifts were greater than the 41-J shifts, reflecting the change in the slope of the CVN curves following irradiation.

Results from the HSSI Sixth Irradiation Series on crack-arrest toughness indicate no irradiation-induced curve shape changes in the K_{Ia} curve. Similar shifts were measured at the 41-J (30-ft·lb) level for CVN specimens and the 100-MPa$\sqrt{m}$ (91-ksi$\sqrt{in.}$) level for K_{Ia} (Ref. 25). Figure 17 shows a comparison of the fracture toughness and crack- arrest toughness for the combined irradiated data for 72W and 73W normalized to the RT_{NDT}. The mean irradiated K_{cl} curve has been shifted much closer to the irradiated K_a curve than is the case for the unirradiated

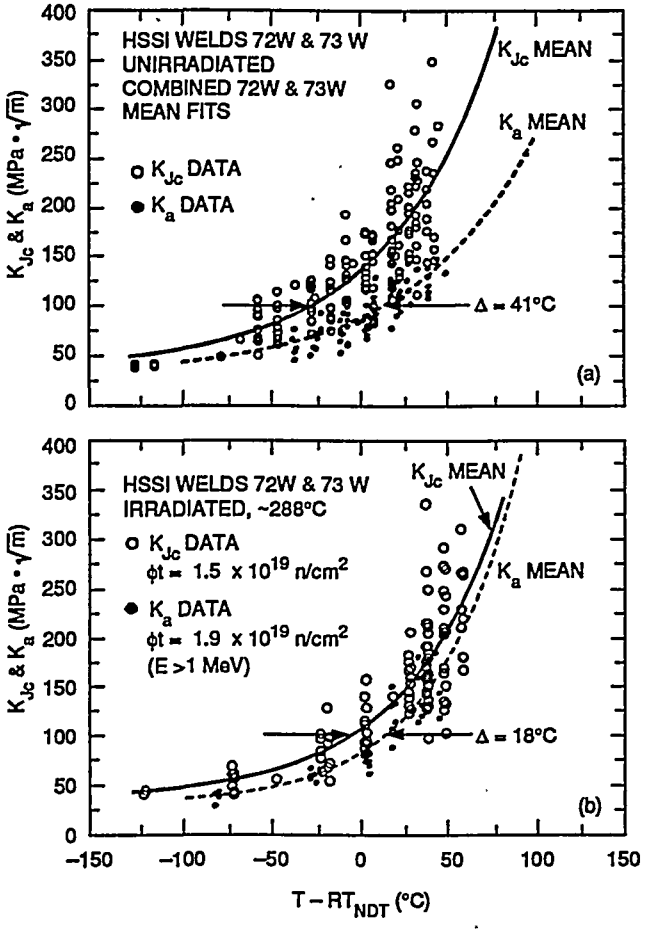

Figure 17 Comparison of mean fracture toughness and crack-arrest toughness vs normalized temperature for welds 72 and 72W in (*a*) unirradiated and (*b*) irradiated conditions.

conditions. The fact that the average separation in initiation and arrest toughness at any given temperature is reduced in the irradiated condition may help explain the enhanced propensity for pop-in events following irradiation.

3.2 Irradiation Embrittlement in a Commercial LUS Weld

The HSSI Program includes examination of the fracture resistance of low-upper-shelf (LUS) welds. This class of submerged-arc welds was produced using Linde 80 welding flux because it produced a very fine dispersion of inclusions within the weld and a resultant low number of reportable defects observed by radiography. Unfortunately, this fine dispersion of inclusions provided such a large number of microvoid initiation sites that the macroscopic resistance of these welds to ductile crack extension by the microvoid growth and coalescence process was significantly reduced. This fine inclusion dispersion, in combination with the common early practice of using copper-coated welding wire, has resulted in a significant number of pressure vessels in which major fabrication welds have both relatively low resistance to ductile fracture in the unirradiated condition and a high sensitivity to further degradation from neutron exposure.

The principal current activity within the HSSI Program to examine LUS welds is the Tenth Irradiation Series. The effects of irradiation on the fracture toughness of commercially fabricated LUS submerged-arc welds from the RPV of the canceled Midland Unit 1 nuclear plant are being investigated. The welds from the Midland plant carry the Babcock and Wilcox Company designation WF-70, a specific combination of weld wire and welding flux that exists in several commercial pressurized-water reactors. The initial part of this study involved the determination of variations in chemical composition, RT_{NDT}, tensile properties, and fracture toughness throughout the welds.[26] Four 1.17-m-long (46-in.) sections of beltline weld and two similar sections of nozzle course weld have been examined. NDT temperatures ranged from –40 to –60°C (–40 to –76°F). Because the Charpy impact energy did not achieve 68 J (50 ft·lb) at NDT + 33°C (59°F), the RT_{NDT} values are all controlled by the Charpy behavior. The RT_{NDT} values vary from –20 to 37°C (–4 to +99°F) with position in the vessel (Fig. 18); the upper-shelf energies (USEs) varied from 77 to 108 J (57 to 80 ft·lb). Analysis of the combined data revealed a mean 41-J (30-ft·lb) temperature of –8°C (18°F) with a mean USE of 88 J (65 ft·lb). Even though both welds carry the WF-70 designation, their bulk copper contents range widely from 0.21 to 0.34 wt % and 0.37 to 0.46 wt % in the beltline and nozzle course weld, respectively.

Tensile and fracture toughness properties were determined on nozzle and beltline weld metals at six temperatures ranging from -100 to 288°C (-148 to 550°F). The yield

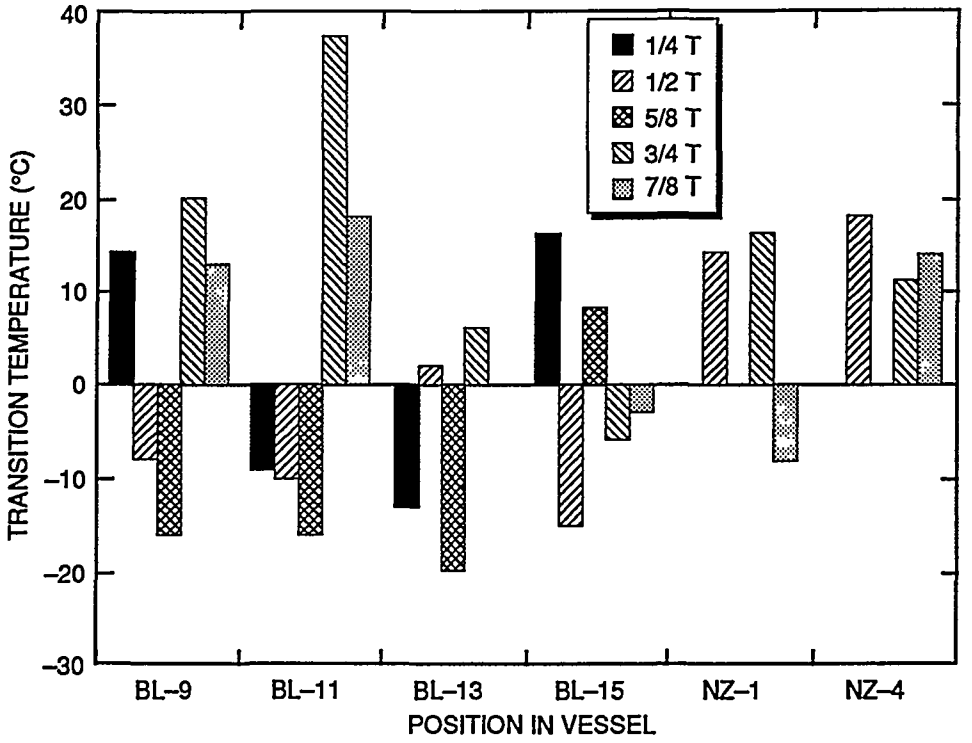

Figure 18 Distribution of RT_{NDT} values for different sections of Midland LUS beltline (BL) and nozzle (NZ) course welds as function of through-thickness position.

strength of the nozzle weld metal was significantly higher than that of the beltline weld, on the order of 100 MPa (14.5 ksi). All the fracture toughness tests to characterize the unirradiated material, using compact specimens ranging up to 101 mm (4 in.) in thickness, have been completed. Data to characterize ductile-to-brittle transition temperature were evaluated using a test standard currently under development by ASTM. This involves the determination of the position of a median fracture toughness transition curve (master curve), using only the data from six 12.5-mm-thick (0.5-in.) (1/2T) compact specimens, to compare with data from large specimens. The "reference temperature" for the master curve was found to be –60°C (–76°F) for the beltline weld and –43°C (–45°F) for the nozzle weld. This appears to agree well with the fact that the mean fracture toughness vs temperature behavior for the beltline weld is higher than for the nozzle weld (Fig. 19).

The irradiation of the Midland weld is in progress. The exposure of the first of the two large irradiation capsules, containing tensile, CVN, and fracture toughness specimens, to the primary target fluence of 1×10^{19} neutrons/cm^2 (E > 1 MeV) has been completed, and the second one has begun. Small fracture toughness and CVN specimens are also being exposed in low- and high-fluence scoping capsules to 5×10^{18} and 5×10^{19} neutrons/cm^2 to examine fluence effects over this range.

4 Interim Conclusions

- The lower-bound fracture toughness for A 533 B plate and weld metal is similar for both shallow- and deep-flaw data sets.
- Data scatter and mean values of fracture toughness are higher for shallow flaws than for deep flaws.
- NDT appears to be a better normalizing parameter than RT_{NDT} for shallow-flaw fracture toughness data.
- The ORNL biaxial specimen permits the effects of biaxial loading on shallow-flaw fracture toughness to be isolated and measured.
- Biaxial loading can produce reductions in the shallow-flaw fracture toughness that can be as high as 40% for equibiaxial loading.

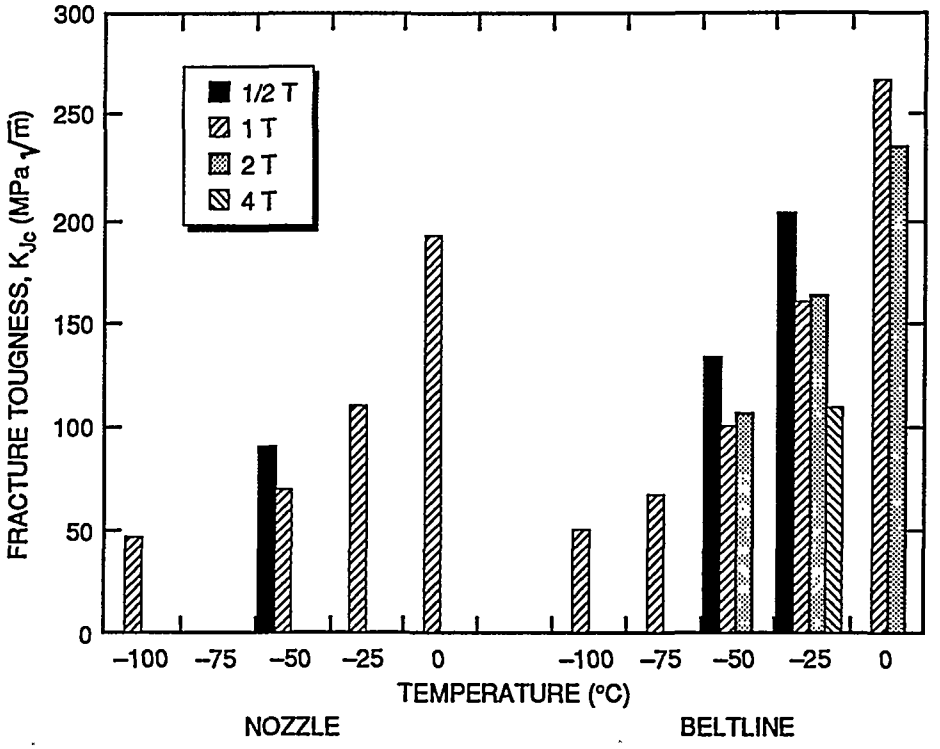

Figure 19 Mean values of unirradiated transition-temperature-range fracture toughness of Midland LUS beltline and nozzle course welds as function of test temperature and specimen size.

- Stress-based dual-parameter fracture toughness correlations cannot predict the observed effects of biaxial loading on shallow-flaw fracture toughness.
- An implicit strain-based dual-parameter fracture toughness correlation has been developed using K_{Jc} and ln(R) as the parameters.
- The K_{Jc}-ln(R) fracture toughness correlation performed acceptably when applied to the uniaxial and biaxial shallow-flaw fracture toughness data.
- Wide ranges in initial fracture properties are observed in some vessel materials, and the current method using CVN-based indices may not be adequately conservative to account for irradiation-induced shifts in fracture toughness.
- Wide ranges of initial chemistry and fracture properties are found in nominally uniform material within a pressure vessel.

References

1. U. S. Nuclear Regulatory Commission, Regulatory Guide 1.99, "Radiation Embrittlement of Reactor Vessel Materials, Enclosure 3, Regulatory Analysis," Rev. 2, November 1987.
2. T. H. Theiss and D. K. M. Shum, Martin Marietta Energy Systems, Inc., Oak Ridge National Laboratory, "Experimental and Analytical Investigation of the Shallow-Flaw Effect in Reactor Pressure Vessels," USNRC Report NUREG/CR-5886 (ORNL/TM-12115), July 1992.
3. J. A. Keeney, B. R. Bass, W. J. McAfee, and S. K. Iskander, Martin Marietta Energy Systems, Inc., Oak Ridge National Laboratory, "Preliminary Assessment of the Fracture Behavior of Weld Material in Full-Thickness Clad Beams," USNRC Report NUREG/CR-6228 (ORNL/TM-12735) (in process).
4. R. E. Link and J. A. Joyce, "Experimental Investigation of Fracture Toughness Scaling Models," *Constraint Effects in Fracture: Theory and Applications*, ASTM STP 1244, M. Kirk and A. Bakker, Eds., 1994.
5. *American Society of Mechanical Engineers Boiler and Pressure Vessel Code*, Sect. III, Div. 1, Paragraph NB-2331, July 1992.
6. T. J. Theiss et al., Martin Marietta Energy Systems, Inc., Oak Ridge National Laboratory, "Initial Results of the Influence of Biaxial Loading on Fracture Toughness," USNRC Report NUREG/CR-6036 (ORNL/TM-12349), June 1993.

7. B. R. Bass, J. W. Bryson, T. J. Theiss, and M. C. Rao, Martin Marietta Energy Systems, Inc., Oak Ridge National Laboratory, "Biaxial Loading and Shallow Flaw Effects on Crack-Tip Constraint and Fracture Toughness," NUREG/CR-6132 (ORNL/TM-12498), January 1994.

8. R. H. Dodds Jr., T. L. Anderson, and M. T. Kirk, "A Framework to Correlate a/W Ratio Effects on Elastic-Plastic Fracture Toughness (Jc)," *International Journal of Fracture*, 48, 1–22 (1991).

9. N. P. O'Dowd and C. F. Shih, "Family of Crack-Tip Fields Characterized by a Triaxiality Parameter: Part 1 – Structure of Fields," *J. Mech. Phys. Solids*, 39, 989–1015 (1991).

10. N. P. O'Dowd and C. F. Shih, "Two Parameter Fracture Mechanics: Theory and Applications," USNRC Report NUREG/CR-5958 (CDNSWC/SME-CR-16-92), Brown University, February 1993.

11. J. W. Hutchinson, "Singular Behavior at the End of a Tensile Crack in a Hardening Material," *J. Mech. Phys. Solids*, 16, 13–31 (1968).

12. J. R. Rice and G. F. Rosengren, "Plane Strain Deformation Near a Crack-Tip in a Power-Law Hardening Material," *J. Mech. Phys. Solids*, 16, 1–12 (1968).

13. R. O. Richie, J. F. Knott, and J. R. Rice, "On the Relationship Between Critical Tensile Stress and Fracture Toughness in Mild Steel," *J. Mech. Phys. Solids*, 21, 394-410 (1973).

14. D. Aurich, "The Influence of the Stress State on the Plastic Zone Size," *Eng. Frac. Mech.* 7, 761–765 (1975).

15. W. E. Pennell, "Heavy-Section Steel Technology Program: Recent Developments in Crack Initiation and Arrest Research," *Nucl. Eng. Des.* 255–266 (1993).

16. D. P. Clausing, "Effect of Plastic-Strain State on Ductility and Toughness," *International Journal of Fracture Mechanics* 6 (1), 71 (March 1970).

17. J. M. Barsom, "Relationship Between Plane-Strain Ductility and K_{Ic} for Various Steels," *Journal of Engineering for Industry* (November 1971).

18. J. G. Merkle, Union Carbide Corp. Nucl. Div., Oak Ridge National Laboratory, "An Elastic-Plastic Thick-Walled Hollow Cylinder Analogy for Analyzing the Strains in the Plastic Zone Just Ahead of a Notch Tip," ORNL-TM-4071, January 1973.

19. V. Weiss, "Material Ductility and Fracture Toughness of Metals," *Proceedings of the International Conference on Mechanical Behavior of Materials, Kyoto, Japan, August 15–20, 1971*, The Society of Materials Science, Japan, 1972.

20. G. P. Gibson, M. Capel, and S. G. Druce, "Effect of Heat Treatment on the Fracture Toughness Transition Properties of an A508 Class 3 Steel, Defect Assessment in Components—Fundamentals and Applications," ESIS/EGF9 (J. G. Blauel and K. H. Schwalbe, Eds.), Mechanical Engineering Publications, London, 1991, pp. 587–611.

21. A. S. Tetleman and A. J. McEvily Jr., *Fracture of Structural Materials*, John Wiley & Sons, Inc., New York, 1967.

22. J. M. Steichen and J. A. Williams, Hanford Engineering Development Laboratory, "High Strain Rate Tensile Properties of Irradiated ASTM A533 Grade B, Class 1, Pressure Vessel Steel," HEDL-TME 73–74, UC-78, July 1973.

23. R. K. Nanstad et al., Martin Marietta Energy Systems, Inc., Oak Ridge National Laboratory, "Irradiation Effects on Fracture Toughness of Two High-Copper Submerged-Arc Welds, HSSI Series 5," USNRC Report NUREG/CR-5913 Vol. 1 (ORNL/TM-12156/V1), October 1992.

24. K. Wallin, "The Scatter in K_{Ic} Results," *Eng. Frac. Mech.* 19(6), 1085–1093 (1984).

25. S. K. Iskander, W. R. Corwin, and R. K. Nanstad, Martin Marietta Energy Systems, Inc., Oak Ridge National Laboratory, "Results of Crack-Arrest Tests on Two Irradiated High-Copper Welds," USNRC Report NUREG/CR-5584 (ORNL/TM-11575), December 1990.

26. R. K. Nanstad et al., Martin Marietta Energy Systems, Inc., Oak Ridge National Laboratory, "Chemical Composition and RTNDT Determinations for Midland Weld WF-70," USNRC Report NUREG/CR-5914 (ORNL-6740), December 1992.